ELSEVIER

Journal of Power Sources 92 (2001) 1–8

JOURNAL OF POWER SOURCES

www.elsevier.com/locate/jpowsour

# In situ X-ray diffraction and X-ray absorption studies of high-rate lithium-ion batteries

M. Balasubramanian, X. Sun, X.Q. Yang, J. McBreen*

*Materials and Chemical Sciences Division, Department of Applied Science, Brookhaven National Laboratory, Upton, NY 11973, USA*

Received 24 December 1999; accepted 2 April 2000

**Abstract**

A combination of in situ synchrotron X-ray diffraction (XRD) and X-ray absorption spectroscopy (XAS) was used to study a two-electrode lithium-ion cell made from electrodes from a high-rate lithium-ion battery. The cathode was $LiNi_{0.85}Co_{0.15}O_2$. Both the XRD and the XAS were done in the transmission mode. XAS was done while the cell was charged at the C/2 rate to 4.5 V. The near edge Co and Ni spectra (XANES) indicated that all of the charge compensation occurred on the Ni and the Co did not change its oxidation state during charge. The Co EXAFS indicated that the Co is randomly distributed in the $NiO_2$ layers. XRD data were collected on a beam line with a position sensitive detector. Complete high quality XRD patterns could be obtained in as little as 3 min. The patterns covered the range between the (0 0 3) and the (1 1 3) reflections of the cathode material and included the (0 0 2) reflection from graphite in the anode. Data were collected while the cell was cycled at rates between the C/4 and 2C rate. In all cases, at the beginning of charge, there is an initial expansion along the *c*-axis and a concomitant contraction along the *a*- and *b*-axes. Towards the end of charge there is a contraction along the *c*-axis and a slight expansion along the *a*- and *b*-axes. After high rate charges there are relaxation processes that last for a few minutes after termination of charge. The results indicate with proper choice of the active materials and electrode design lithium-ion cells can be charged and discharged at high rate with high utilization of the active material. 

*Keywords:* Lithium ion; Batteries; X-ray diffraction; X-ray absorption spectroscopy

## 1. Introduction

Batteries with power-to-energy ratios greater than 20 kW $kW^{-1}$ $h^{-1}$ are required for hybrid vehicles. The primary functions of the battery are to load-level the dynamic loads during acceleration, and to a limited degree, hill-climbing and to recapture the energy lost during braking. The lithium-ion battery is a candidate for this application. High power requires the use of high surface area active materials and thin electrode construction. The behavior of lithium-ion batteries and their degradation mechanisms in these applications are unknown. In the United States work on these batteries is being conducted by industrial battery developers under the combined sponsorship of the United States Department of Energy (DOE) and the United States Automotive Battery Consortium (USABC). Several national laboratories are doing diagnostic work to elucidate degradation mechanisms. One of the industrial developers (PolyStor Corp.) has built high rate 18650 lithium-ion cells and delivered them to the national laboratories. At Brookhaven National Laboratory (BNL) we have disassembled these cells and punched electrodes from the cathodes and anodes. These electrodes were assembled in spectroelectrochemical cells. The work included both in situ X-ray diffraction (XRD) and X-ray absorption spectroscopy (XAS) studies. The combination of XRD and XAS is a very powerful technique for the study of electrode processes. XRD can identify phase transitions in both cathodes and anodes and XAS gives information on the chemistry and redox processes on the transition metals in the cathodes.

## 2. Experimental

### 2.1. The 18650 cells

The 18650 lithium-ion cell had a spirally wound cell pack. The cathode formulation was coated on both sides of a 30 μ Al current collector and the anode formulation was coated on both sides of a 15 μ Cu current collector. The separator was a 37 μ microporous polyethylene membrane and the electrolyte was 1 M $LiPF_6$ in a 1:1 EC:DMC solvent. The

* Corresponding author. Tel.: +1-631-344-4513; fax: +1-531-344-4071.
*E-mail address*: jmcbreen@bnl.gov (J. McBreen).

0378-7753/01/$ – see front matter 
PII: S0378-7753(00)00493-6

cathode active material was lithium nickel cobalt oxide (Sumitomo). The chemical analysis from the supplier indicated a composition $Li_{1.023}Ni_{0.872}Co_{0.151}O_{2.05}$. The cathode formulation was 84% (all percentages are in terms of weight) active material, 4% acetylene black, 4% graphite flake (Timcal SFG-6) and 8% PVDF binder (Kureha KF-1100). The anode formulation was 75% carbon (Osaka Gas MCMB-6-2800), 16.5% graphite flake (Timcal SFG-6) and 8.5% PVDF binder (Kureha #c).

The manufacturer had given the cells formation cycles and delivered the cells in the discharged state. The cell was disassembled under an argon atmosphere in a glove bag and the cell pack was sealed in a polypropylene bottle and each bottle was sealed in a larger bottle for double protection. The bottles were then transferred to a glove box with an argon atmosphere. All the remaining steps for assembling the spectroelectrochemical cells were done in the glove box.

### 2.2. The spectroelectrochemical cell

Fig. 1 shows a schematic of the spectroelectrochemical cell. Discs (1.8 cm diameter) were punched from the anodes and cathodes of the disassembled cells. The active material was removed from one side of the current collector prior to assembly in the cell. The cell pack consisted of the anode, cathode, a fresh Celgard separator and electrolyte (1 M $LiPF_6$ in a 1:1 EC:DMC solvent). The cell was housed between two machined blocks of aluminium. The aluminium blocks were machined to provide X-ray windows and holes for bolts. The windows were sheets of 250 μ Mylar. A rubber gasket was used to make a hermetic seal. Provisions were made for current collection by using thin strips of copper and aluminium.

### 2.3. X-ray absorption

In situ XAS experiments were done in the transmission mode using methods described elsewhere [1]. The measurements were done at beam line X11A at NSLS. XAS scans covering both the Co and Ni K edges were taken while charging the cell at the C/2 rate. A third ionization chamber was used in conjunction with Co and Ni foils to provide internal calibration for the alignment of the edge positions. A total of seven scans were taken during charge.

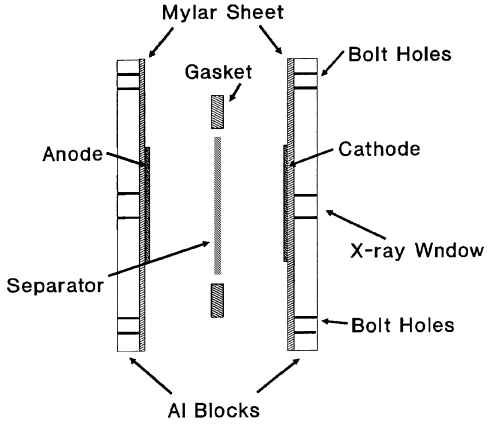


Fig. 1. The spectroelectrochemical cell.

### 2.4. X-ray diffraction

In situ XRD studies were done in the transmission mode at Beam Line X7A at the National Synchrotron Light Source (NSLS). The general procedures for in situ XRD are described in previous publications [2–4]. The XRD facility at X7A is particularly suitable for collecting data at fast rates with high resolution [5]. This is due to the use of a position sensitive detector (PSD), developed at BNL [6].

In collecting data in the transmission mode the X-ray beam has to pass through the lithium nickel cobalt oxide and the 15 μ Cu foil current collector. Co, Ni and Cu are adjacent first row transition metals with their respective K absorption edges at 7709, 8333 and 8979 eV. To minimize absorption, the X-rays should have an energy that is either below the Co K edge or a higher energy beyond the Cu K edge where the absorption is equally low. The X-ray absorption by the cathode is almost identical at 7.5 and 17 keV. In the present work the beam energy was 17.688 keV (0.7009 Å). Because of the inverse relationship between the $d$-spacings and $2\theta$, the X-ray pattern is compressed. However, with the PSD it is possible to collect high-resolution data at fast rates. The PSD is a multiwire proportional device that is operated with a 90% Kr–10% $CO_2$ gas mixture at 4 bar. Data collection at 17.688 keV, which is above the Kr edge, increases the spatial resolution of the detector [5,6].

## 3. Results and discussion

### 3.1. X-ray absorption

#### 3.1.1. X-ray absorption

Excellent X-ray absorption spectra were obtained at both the Co and Ni K edges. This was due to the high uniformity of the manufactured cathode and to an almost ideal loading of the material for a XAS experiment. The respective step heights at the Co and Ni edges were 0.27 and 1.29. Analysis of the data, using the McMaster Table [7], indicated a weight ratio of Ni:Co of 5.4:1, which is close to the weight ratio of 5.7:1 based on the reported chemical analysis. The step heights indicated a cathode active material loading of 8.64 mg $cm^{-2}$. Assuming a capacity of 180 mA h $g^{-1}$, this yields a nominal capacity density of 1.56 mA h $cm^{-2}$, or an electrode capacity of 4 mA h. This agrees reasonably well with the electrochemically determined capacities of the spectroelectrochemical cells.

#### 3.1.2. XANES

Fig. 2 shows a charging curve for the cell when charged at the C/2 rate. The figure also indicates where the XAS spectra

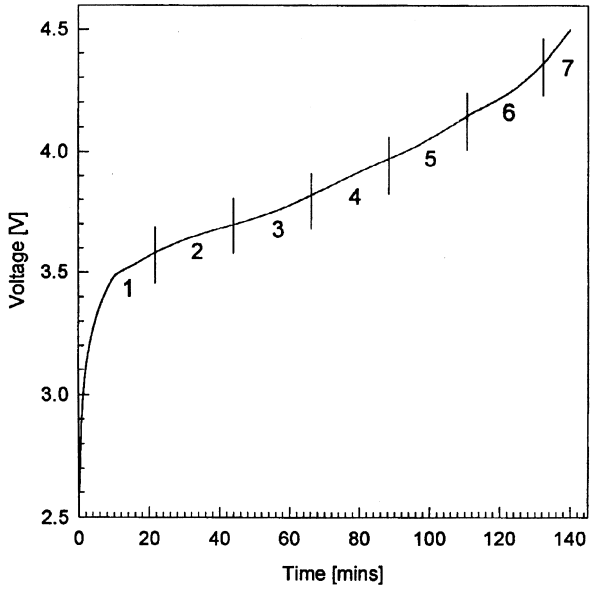


Fig. 2. Charging curve for the spectroelectrochemical cell during the XAS measurements. The cell was charged at 2 mA (C/2 rate). The XAS scans are indicated on the curve.

were taken during the charge. Fig. 3 shows the X-ray absorption near edge structure (XANES) at the Ni K edge. During charge the edge position of the first five scans shifts to higher energies. There is no further shift in edge position during the last two scans. Fig. 4 shows the XANES at the Co K edge. There is very little shift in the Co edge. In a separate

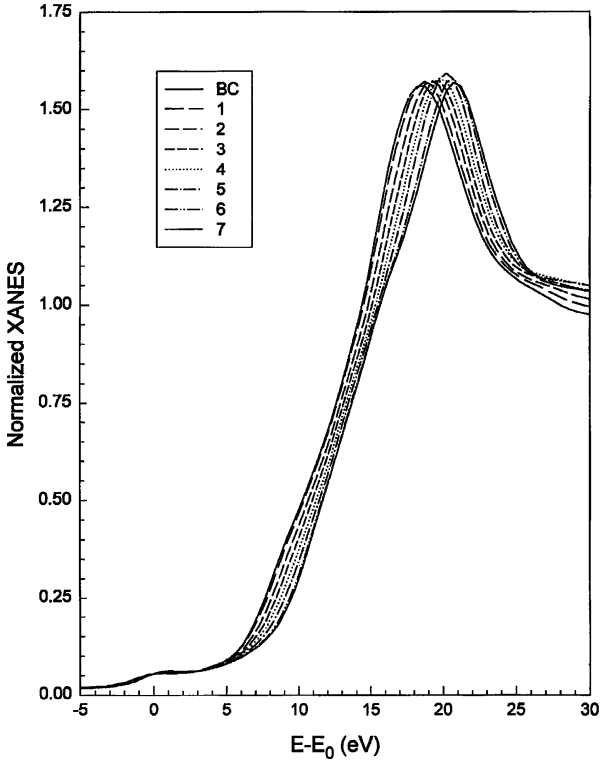


Fig. 3. Ni K edge XANES, before charge (BC) and during charge [1–7].

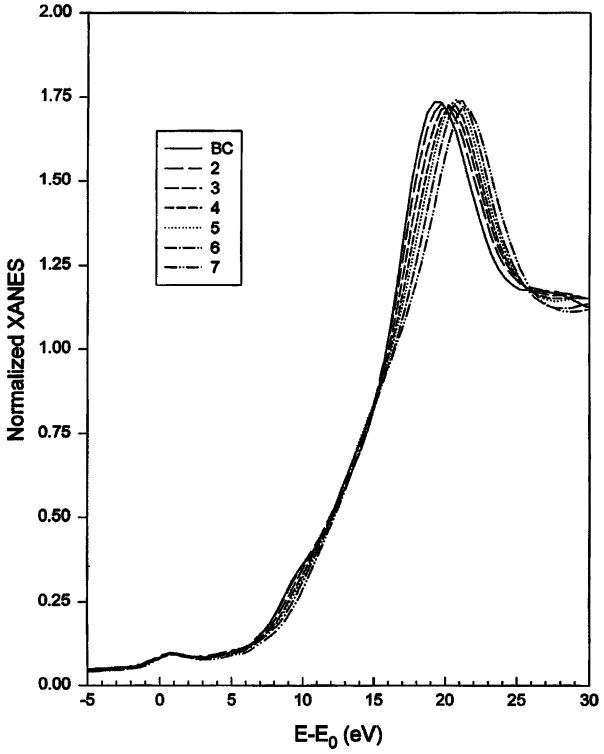


Fig. 4. Co K edge XANES, before charge (BC) and during charge [2–7].

study we have done in situ XAS while charging the Sumitomo material at the C/10 rate to 5.1 V in a cell with a Li foil anode. Slight shifts were seen in at the Co edge in the voltage range of 4.5 to 5.1 V. The Ni K edge continuously shifted up to a voltage of 4.5 V. There was no further movement of the edge between 4.5 and 5.1 V. This indicates that during cathode delithiation charge compensation occurs first on the Ni and then on the Co. With the lower voltage cut-off of 4.5 V it appears that little or none of the Co is oxidized to Co(IV) and the charge compensation occurs mostly on the Ni. Nakai and Nakagome have reported XANES results for $Li_{1-x}Ni_{0.5}Co_{0.5}O_2$ charged to a composition of $x$=0.8 [8]. Their results indicate that charge compensation occurs on the Ni up to $x$=0.5 and beyond that composition there is no further change in the Ni K edge position.

### *3.1.3. EXAFS*

Fig. 5 shows Fourier transforms of the Ni EXAFS. Here we only present a preliminary qualitative analysis of the data because the Cu foil limits the range of the Ni EXAFS. A complete analysis of the EXAFS from the cell with the Li foil anode will be given in a subsequent paper. The Fourier transforms are uncorrected for photoelectron phase shifts; thus the quoted bond distances are ~0.3–0.4 Å shorter than the actual bond distances. The peaks at ~1.5 Å are due to the Ni–O interactions of the first coordination shell. The amplitude of these peaks increases with the degree of charge. This is due to a dynamic Jahn–Teller distortion for Ni(III) [9,10]. When Ni is oxidized to Ni(IV) during charge the oxygen

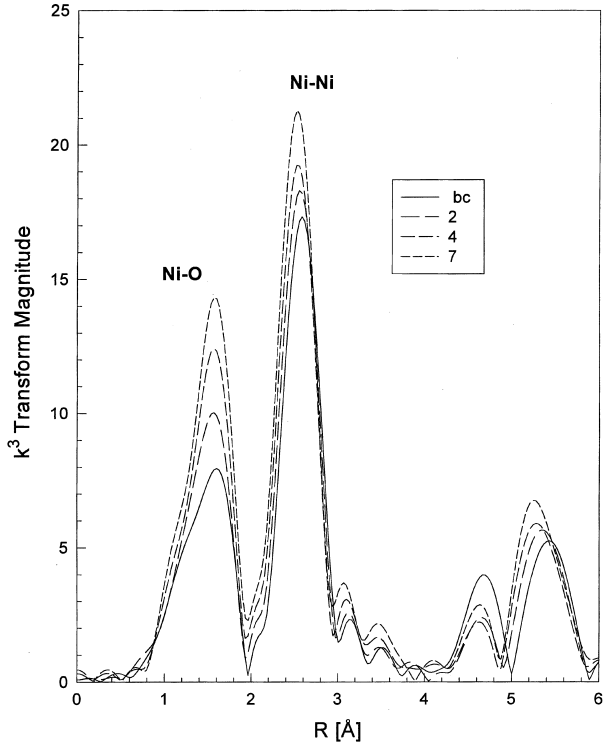


Fig. 5. Fourier transform of Ni EXAFS, before charge (BC) and selected scans (2, 4 and 7) during charge. $\Delta k$=3–12 Å$^{-1}$, $k^3$ weighted.

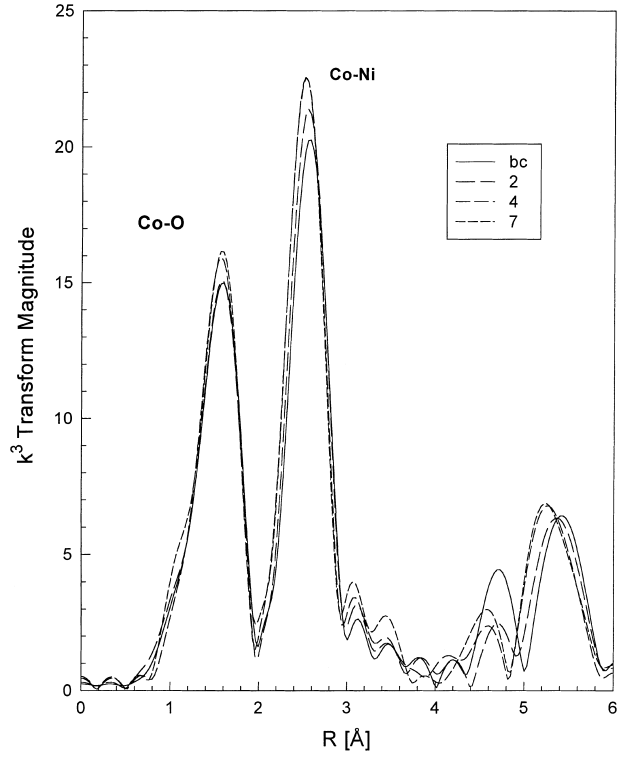


Fig. 6. Fourier transform of Co EXAFS, before charge (BC) and selected scans (2, 4 and 7) during charge. $\Delta k$=3–12 Å$^{-1}$, $k^3$ weighted.

coordination around the Ni becomes symmetrical and the peak magnitude increases. The second set of peaks, at ~2.6 Å, is due to the first Ni–Ni coordination shell in the basal plane. The shifts to lower $R$ values during charge are due to a contraction in the Ni–Ni bond distances. The peaks at ~5.4 Å are due to backscattering by a second coordination shell of Ni atoms that are aligned with the Ni atoms of the first Ni–Ni shell and are at double the distance of the first shell. This alignment produces a forward scattering effect that yields peaks in the Fourier transform at large $R$.

Fig. 6 shows Fourier transforms of the Co EXAFS. There are very little changes in the magnitude of the Co–O peaks because Co(III) is not a Jahn–Teller active ion. The behavior of other peaks in the Fourier transform is very similar to that of the Ni EXAFS. This is quite different to the behavior of the Co EXAFS for $LiCoO_2$ [11]. The position of the two Co–Co peaks in $Li_{1-x}CoO_2$ does not change with state of charge. Furthermore, the transform magnitude for both first and second Co–Co peaks decrease with increasing state of charge. This apparently is due to disorder in the $CoO_2$ layers. In the mixed oxide the behavior of the two Co-metal (Ni and Co) shells is more like that found for $LiNiO_2$ [10]. There is a decrease in $R$ and an increase in the magnitude of the peaks with charge. These results indicate that the Co is randomly distributed in the $NiO_2$ layers. There was a recent report on in situ Co XAS on $LiNi_{0.8}Co_{0.2}O_2$ [12]. In that investigation they also observed a shrinkage in the Co next-nearest neighbor metal–metal bond lengths during charge. They attributed the effect to a change in the Co oxidation state. Based on the XANES results at the Ni and Co K edges we attribute the bond shrinkage to contractions induced in the host lattice by oxidation of Ni.

### 3.2. X-ray diffraction

#### 3.2.1. X-ray diffraction

Table 1 lists the cycling conditions under which in situ XRD scans were collected. Most of the XRD data presented in this paper will be confined to second charge at the C/2 rate to 4.5 V and the fourth charge at the 2C rate from 50% state of charge (SOC) to 4.5 V. Fig. 7 shows the XRD pattern for the cell on open circuit before the first charge. The reflections for the lithium nickel cobalt oxide are indexed. There are also reflections for the Cu and Al current collectors. The (0 0 2) graphite reflection can be seen at 11.9°. The broad diffuse features between 7° and 13° and around 20° are due to scattering by the separator, the binder and the Mylar windows.

#### 3.2.2. Second charge at C/2 rate

Fig. 8(a) shows the charging curve on the second cycle when the cell was charged at the C/2 rate. The times when the XRD scans were recorded are indicated on the charging curve. The charge ended close to the end of the 11th scan. The complete XRD scans are shown in Fig. 9. The graphite (0 0 2) reflection moves to lower angles as charge progresses. This clearly indicates that the reflection comes from the anode material and indicates the expansion

Table 1
Cycling conditions for in situ XRD studies[a]

| Cycle No. | Charge/discharge | Current (mA) | Charge/discharge limit | Capacity (mA h) |
|---|---|---|---|---|
| 1 | Charge | 0.8 | 4.5 V | |
| | Discharge | 0.8 | 2.5 V | −4.29 |
| 2 | Charge | 2.0 | 4.5 V | +4.28 |
| | Discharge | 2.0 | 64 min (3.65 V) | −2.13 |
| 3 | Charge | 4.0 | 4.5 V | +2.02 |
| | Discharge | 4.0 | 30 min (3.55 V) | −2.00 |
| 4 | Charge | 8.0 | 4.5 V | +1.80 |
| | Discharge | 8.0 | 2.1 V | −3.33 |
| 5 | Charge | 4.0 | 5.2 V | +4.66 |
| | Discharge | 4.0 | 2.0 V | −3.93 |

[a] The end of discharge voltage for the discharges to 50% SOC are indicated in brackets. The charge capacity is indicated as (+) and the discharge capacity as (−).

along the *c*-axis as lithium is intercalated into the anode. Figs. 10–12 show expanded views of various sections of the spectra. The peaks in the XRD spectra can be indexed to a hexagonal phase similar to that indexed by Yang et al. for $LiNiO_2$ [4]. In Fig. 9 the first scan was obtained immediately after starting the charging process while the last scan (*R*) was obtained at open circuit immediately after the completion of charge. The *c*-axis is normal to the set of planes that contribute to the (0 0 3) and (0 0 6) reflections. Therefore, changes in the *c*-axis can be monitored by inspection of the (0 0 3) and (0 0 6) reflections. In contrast, the (1 1 0) reflection arises from a set of planes that are parallel to the *c*-axis. Therefore, the (1 1 0) reflection is sensitive only to changes in the length of the *a*- or *b*-axes. The other indexed reflections from the cathode material will have contributions from components of the *a*-, *b*- and *c*-axes. It can be seen in Fig. 10 that on charging, the (0 0 3) peak position shifts continuously to lower values and also broadens to a small extent from scans 1–8. This indicates that the *c*-axis expands during initial stages of charge. Yang et al. found that in fresh $LiNiO_2$ a set of new peaks, which they indexed to a new hexagonal phase, emerges at the expense of the original hexagonal phase on charging (between 3.9 and 4.2 V) [4]. The (0 0 3) peak of the newly formed phase occurs at a lower

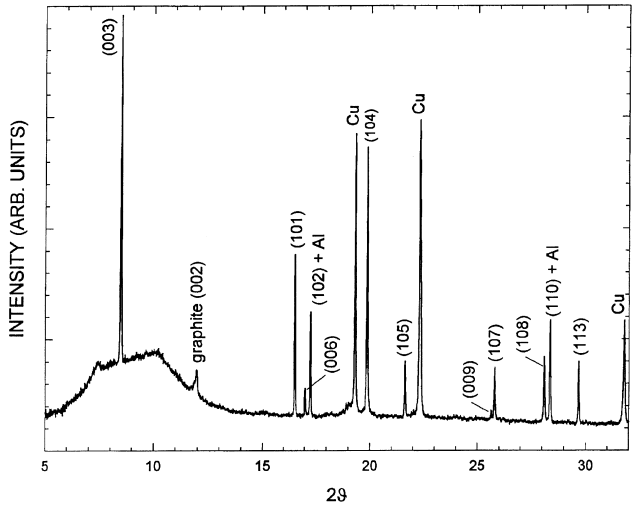


Fig. 7. XRD pattern for cell before beginning of the first charge. The peaks for the lithium nickel cobalt oxide and graphite are indexed. The peaks for the Cu and Al current collectors are also indicated.

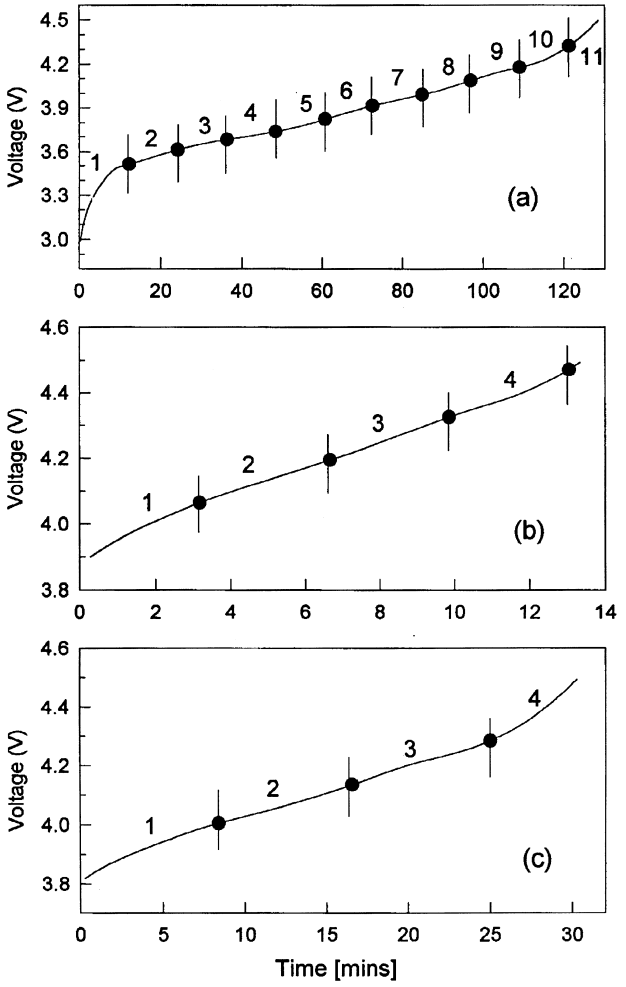


Fig. 8. Charging curves for cell: (a) cycle 1, (b) cycle 4 and (c) cycle 3. The times when the XRD scans were taken are indicated on the curves.

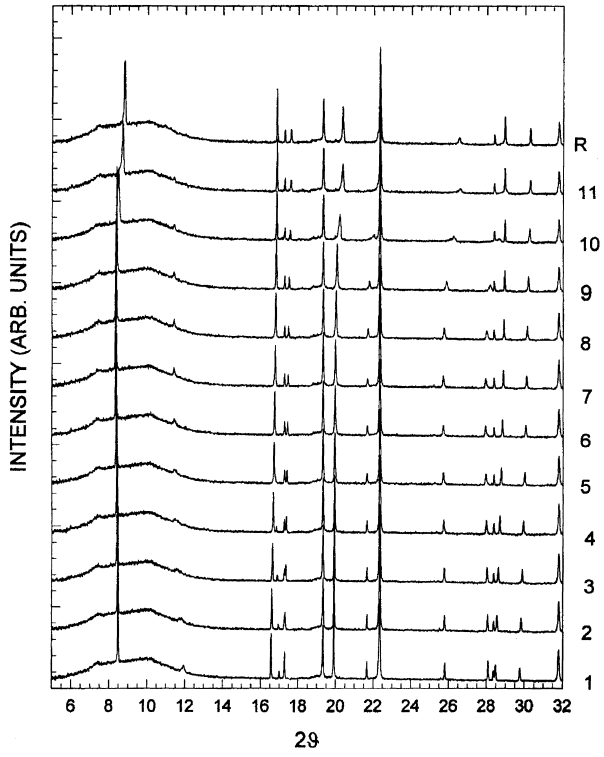


Fig. 9. The XRD patterns recorded during the second charge at the C/2 rate. The charge terminated two-thirds way through scan 11. Scan *R* was obtained on open-circuit immediately after charge.

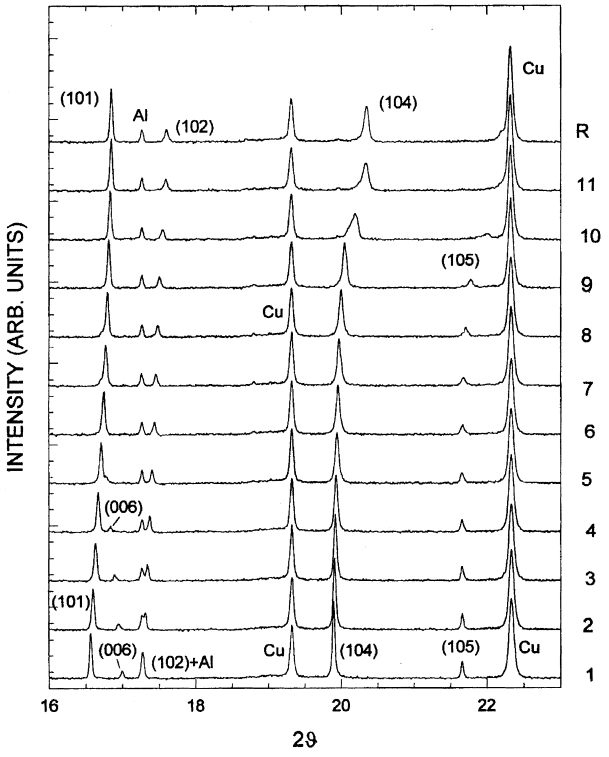


Fig. 11. An expanded view of the XRD patterns in Fig. 9 in the $2\theta$ range of 16–22°.

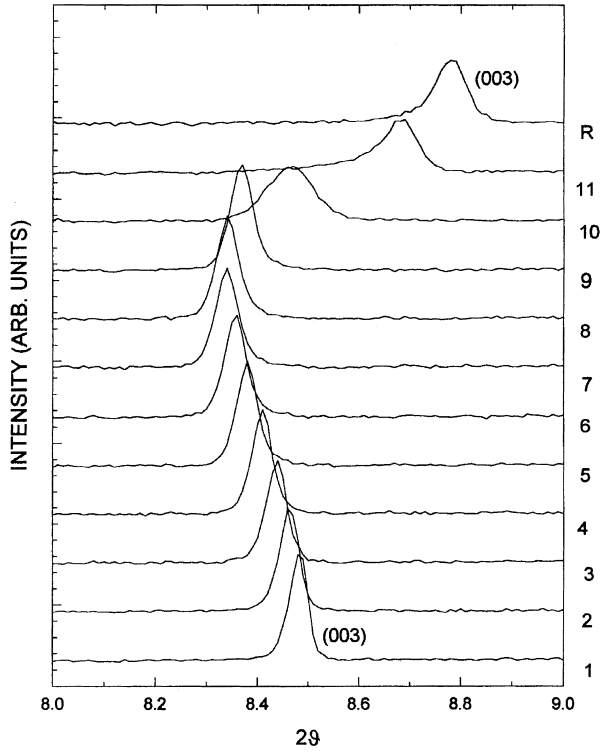


Fig. 10. The (0 0 3) peak recorded during the second charge at the C/2 rate.

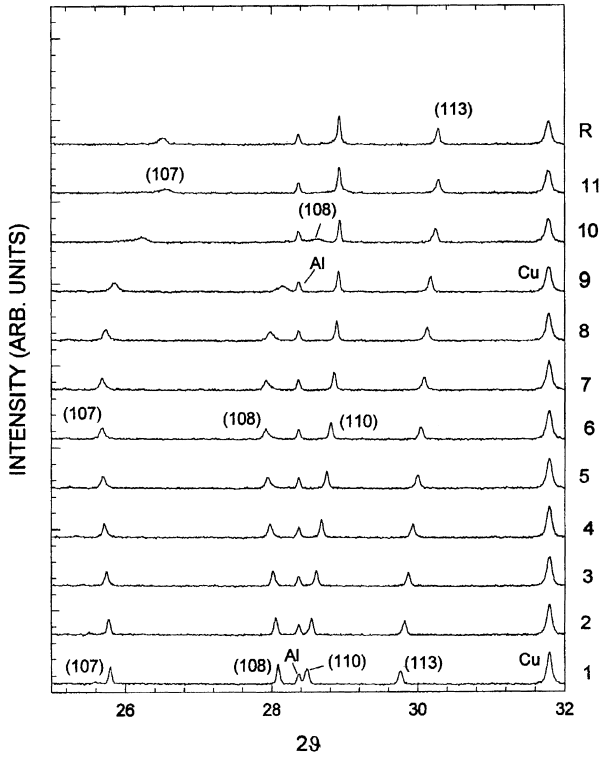


Fig. 12. An expanded view of the XRD patterns in Fig. 9 in the $2\theta$ range of 24–32°.

angle than the original phase, indicating that the newly formed phase has a larger *c*-axis. Unlike fresh $LiNiO_2$, the XRD pattern for the pre-cycled cathode material does not show the formation of a distinct new phase on charging. This behavior is also seen in pre-cycled $LiNiO_2$ electrodes and will be reported elsewhere. Unlike the (0 0 3) peak, the (1 1 0) peak moves to higher angles during scans 1–8, as shown in Fig. 12. One can easily monitor the movement of the (1 1 0) peak by observing its position with respect to the close-by Al peak (which comes from the current collector at the cathode). The shift to higher angles indicates that the *a*- and *b*-axes contract during scans 1–8. From scan 9–11 the (0 0 3) peak shifts to higher angles and broadens significantly. The (1 1 0) peaks show a small tendency to shift to smaller angles. These observations suggest that during these scans the *c*-axis contracts significantly while the *a*- and *b*-axes expand to a small extent. Figs. 9–12 also show a shift in the position of the (10*l*) peaks during charge. The shift in the position of the (10*l*) peaks is intermediate to that of the (0 0 3) and the (1 1 0) peaks. The (10*l*) reflections with larger *l* values, such as (1 0 8), follow the trends seen for the (0 0 3) peaks while those with smaller *l* values, such as (1 0 1) follow the (1 1 0) peak. As the value of *l* increases one expects the contribution from the changes in the *c*-axis length will increase, since the *c*-axis becomes more normal to the (10*l*) planes with larger *l* values. Thus, the shift in the (1 0 8) reflection will be similar to the changes in the (0 0 3) reflection while the shift in the (1 0 1) reflection will more closely follow that of the (1 1 0) reflection. Finally, the trend in the changes in the (0 0 6) reflection is similar to that of the (0 0 3) reflection. The (0 0 6) reflection becomes very weak after scan 5 and cannot be clearly distinguished from the (1 0 1) peak.

### 3.2.3. Fourth charge at the 2C rate

Fig. 8(b) shows the charging curve for the cell when charged from 50% SOC to 4.5 V. The low polarization is indicative of the high rate capability of the cell. The times when XRD scans were recorded are indicated on the charging curve. Fig. 13 shows the complete scans. The end of charge occurred close to the beginning of the fifth scan. The data acquisition time for each scan was 3 min. Because of the fast data acquisition time the data had more noise. However, the signal-to-noise ratio is still very good. The overall behavior of the diffraction peaks is very similar to that seen at the C/2 rate. Fig. 14 shows the (0 0 3) reflection. It clearly shows an initial expansion along the *c*-axis followed by a contraction towards the end of charge. The contraction was much less than that seen when the cell was charged at the C/2 rate (Fig. 10). At the higher charge rate the cell reaches the 4.5 V cut-off at a lower state of charge and less lithium is removed from the cathode. The result is less contraction along the *c*-axis. There was no significant residue from the low angle reflections of the uncharged material in the fifth scan, indicating excellent utilization of the active material at high rates.

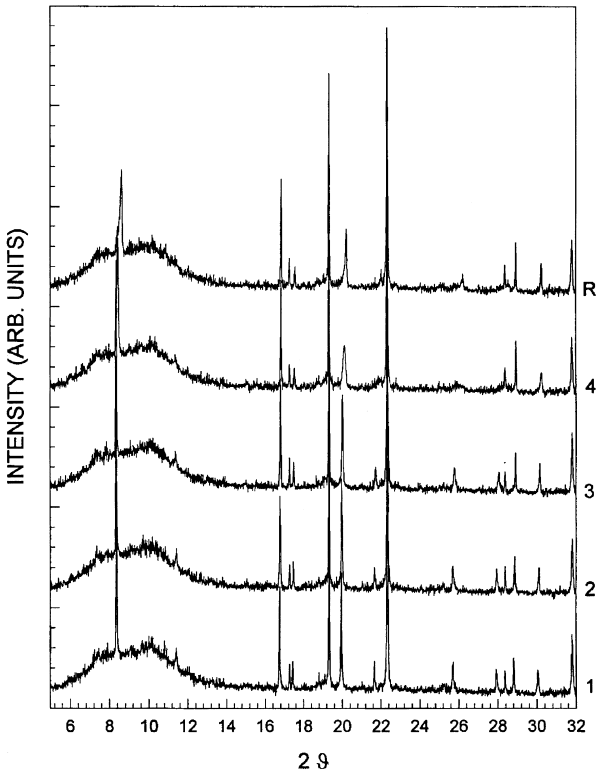


Fig. 13. The XRD patterns recorded during the fourth charge at the 2C rate. The charge terminated close to the beginning of the last scan (*R*).

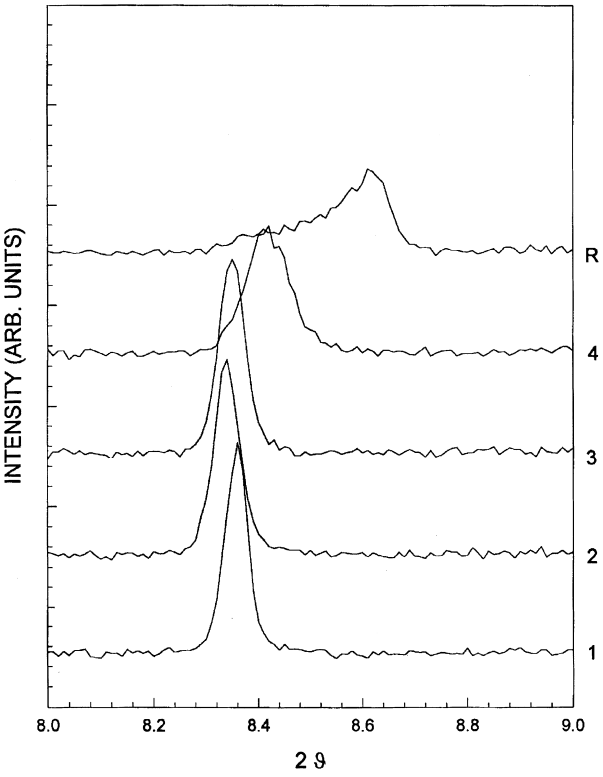


Fig. 14. The (0 0 3) peak recorded during the fourth charge at the 2C rate.

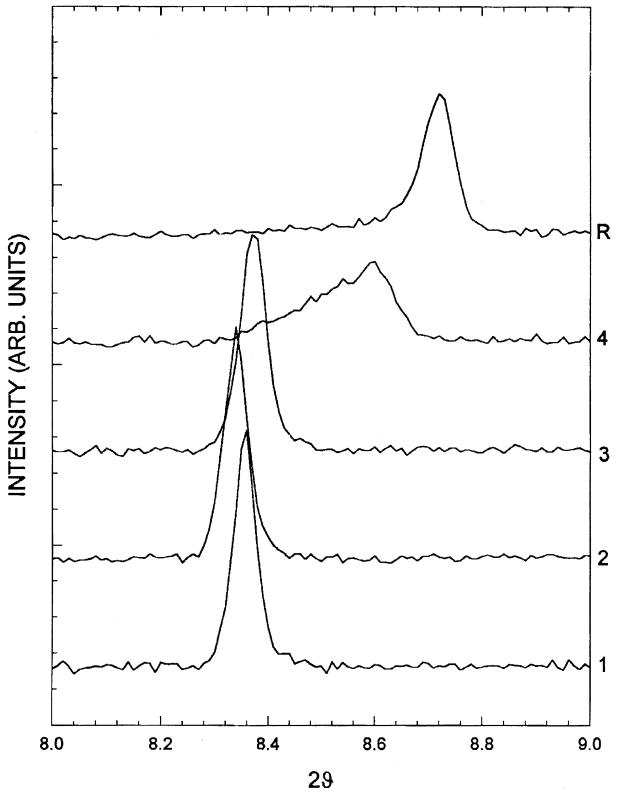


Fig. 15. The (0 0 3) peak recorded during the third charge at the C rate. The charge terminated about two-third way through scan 4. Scan *R* was recorded on open circuit immediately after charge.

Fig. 15 shows the (0 0 3) peak when the cell was charged at the C rate. The charge terminated during the fourth scan. Scan *R*, taken on open-circuit immediately after charge, shows a further shift in the peak. Two subsequent scans (not shown) showed no further peak shifts. This indicates relaxation processes that can last for several minutes after a high rate charge. The contraction along the *c*-axis was intermediate between that found at the C/2 and 2C rates.

## 4. Conclusions

With synchrotron X-rays it is possible to do in situ XAS and XRD, in the transmission mode, on two electrode cells with conventional Al and Cu foil current collectors. XAS results indicate that during charging of $LiNi_{0.85}Co_{0.15}O_2$ to 4.5 V all of the charge compensation occurs on Ni and the oxidation state of the Co does not change. The Co EXAFS results are consistent with a random distribution of Co in the $NiO_2$ layers. By using a beam line with a position sensitive detector it was possible to collect complete high quality XRD spectra, covering a range between the (0 0 3) and (1 1 3) reflections, in as little as 3 min. In situ XRD results on a cell charged at several rates, between the C/4 and 2C, indicate that on charge there is an initial expansion in the cathode material along the *c*-axis and a simultaneous contraction along the *a*- and *b*-axes. Towards the end of charge there is a major contraction along the *c*-axis and a slight expansion along the *a*- and *b*-axes. XRD scans, taken on completion of high rate charges indicate that there are relaxation processes in the cathode, which last for several minutes after termination of charge.

## Acknowledgements

This work was supported by the Assistant Secretary for Energy Efficiency and Renewable Energy, Office of Advanced Automotive Technologies, US Department of Energy under Contract Number DE-AC02-98CH10886. The XAS measurements were done at Beam Line X11A and the XRD measurements were done at Beam Line X7A of NSLS. The authors gratefully acknowledge support of the USDOE, Division of Materials Science, under Contract Number DE-FG05-89ER45384 for its role in the development and operation of Beam Line X11A at the National Synchrotron Light Source (NSLS). The NSLS is supported by the Department of Energy, Division of Materials Science under Contract Number DE-AC02-98CH10886.

## References

[1] M. Giorgetti, S. Passerini, W.H. Smyrl, S. Mukerjee, J. McBreen, J. Electrochem. Soc. 146 (1999) 2387.
[2] T.R. Thurston, N.M. Jisrawi, S. Mukerjee, X.Q. Yang, J. McBreen, M.L. Daroux, X.K. Xing, Appl. Phys. Lett. 69 (1996) 194.
[3] S. Mukerjee, T.R. Thurston, N.M. Jisrawi, X.Q. Yang, J. McBreen, M.L. Daroux, X.K. Xing, J. Electrochem. Soc. 145 (1998) 466.
[4] X.Q. Yang, X. Sun, J. McBreen, Electrochem. Commun. 1 (1999) 227.
[5] A.P. Jephcoat, L.W. Finger, D.E. Cox, High Pressure Res. 8 (1992) 667.
[6] G.C. Smith, Synchrotron Radiation News 3 (1991) 23.
[7] W.H. McMaster, N. Kerrdel Grande, J.H. Mallet, J.H. Hubbel, Compilation of X-ray Cross Sections, National Technical Information Service, Springfield, VA, 1969.
[8] I. Nakai, T. Nakagome, Electrochem. Solid State Lett. 1 (1998) 259.
[9] A. Rougier, C. Delmas, A.V. Chadwick, Solid State Commun. 94 (1995) 123.
[10] A.N. Mansour, J. McBreen, C.A. Melendres, J. Electrochem. Soc. 146 (1999) 2799.
[11] I. Nakai, K. Takahashi, Y. Shiraishi, T. Nakagome, F. Nishikawa, J. Solid State Chem. 140 (1998) 145.
[12] J. Kropf, C.S. Johnson, Abstracts of the Fall MRS Meeting, Boston, MA, 29 November–3 December 1999, Abstract R14.7.